12th International Symposium on Turbulence and Shear Flow Phenomena (TSFP12)
Osaka, Japan (Online), July 19-22, 2022

IMPACT OF GRID RESOLUTION ON HYBRID RANS-LES OF TRANSITION IN A SEPARATED BOUNDARY LAYER

Eike Tangermann
Department of Aerospace Engineering
University of the Bundeswehr Munich
85577 Neubiberg, Germany
eike.tangermann@unibw.de

Markus Klein
Department of Aerospace Engineering
University of the Bundeswehr Munich
85577 Neubiberg, Germany
markus.klein@unibw.de

ABSTRACT

Laminar separation followed by transition and reattachment on a wing at low Reynolds number has been simulated using hybrid RANS-LES (DDES, IDDES) on differently refined meshes. The different stages of this process are investigated with respect to mesh resolution in order to determine their particular requirements with the primary focus on the transition process, for which the development of turbulent fluctuations and their length scales is discussed. For reference DNS data of the flow is presented.

INTRODUCTION

In low Reynolds number flow, boundary layers tend to separate early while still in laminar state. Following the laminar separation on airfoils or similar objects, regions of separated flow occur above which the transition process to turbulent conditions takes place. Often the turbulent fluctuations bring momentum towards the wall and thereby initiate a reattachment of the flow which continues in a fully turbulent boundary layer.

The accurate prediction of this process by numerical simulation is challenging, which mostly depends on the treatment of turbulence in terms of how it is modeled and which part is resolved. Upstream of the separation no turbulence is present and the model needs to account for the laminar flow and remain inactive. Therefore, a supplementary model is necessary which, depending on the turbulence model approach, detects or even predicts the transition process. The range of possible turbulence treatment is very wide in this context. Already RANS can predict the flow at acceptable accuracy if the integral behavior is more important than local details of transition and turbulence (Catalano & Tognaccini (2010)). On the other hand, for low Reynolds numbers and relatively simple geometries LES and even DNS are achievable but still require high computational effort (Galbraith & Visbal (2010)). These turbulence-resolving methods do not only offer a better prediction of the turbulent part of the boundary layer but especially of the transition process.

Hybrid RANS-LES offers an intermediate approach, where the flow close to the wall is treated by URANS whereas LES is applied further away from the wall. Thereby the transition above the separation bubble is captured by the LES mode as well as the upper part of the boundary layer, which carries most turbulence energy as shown in previous work by the authors (Tangermann & Klein (2021, 2020)). Its benefit is a reduced computational effort while maintaining a good level of accuracy.

For the application of DNS, the grid cell width is prescribed by the smallest turbulent scales. All other approaches which involve modeling turbulence partially or completely allow a coarser cell width within a limited range. In computations using RANS it is very common practice to perform a study of grid dependence and quantify the inaccuracy of the solution induced by the grid resolution. In that case the grid dependence is caused purely by errors induced from the discretization of the flow field. When LES is involved, however, the solution depends not only on errors from discretization but also on modeling errors resulting from the cutoff scale representing the smallest resolved turbulent structures. Since in LES the grid typically is selected relatively fine compared to the structures of the mean flow field, the error from modeling usually has more weight than the one from discretization. Nevertheless, grid dependence studies in LES are very expensive in terms of computational effort and therefore not often performed. The quality of results is rather assured by criteria based on the resolved structures.

In hybrid RANS-LES different criteria of mesh resolution apply depending on the location. Within the present work, hybrid RANS-LES simulations of laminar separation on a NACA0018 airfoil have been performed at 4° angle of attack and a Reynolds number of $Re = 80000$ in order to investigate the impact of grid resolution on the flow prediction. These conditions offer a generous spacing between separation, transition and reattachment and therefore allow for the observation of these phenomena in a more isolated way. For validation and comparison purposes, the hybrid RANS-LES data are supplemented by DNS for reference and 2D URANS results. The latter is considered in order to observe the underlying RANS model of the hybrid simulations individually.

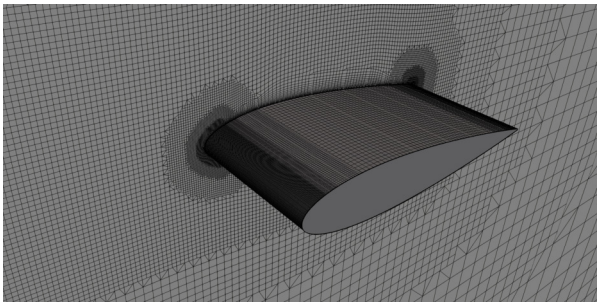

Figure 1: Structure of the mesh around the wing, coarsest mesh.

GEOMETRY AND NUMERICAL SETUP

The wing is a quasi two-dimensional geometry of NACA0018 airfoil. Its extension in span-wise direction b is half the chord length c with periodically coupled planar boundaries. This span allows the solution to develop independently of the periodicity. In the remaining two directions the wing is surrounded by a square shaped farfield boundary which is located 20 times c from the wing. In previous work this distance was found sufficient to keep the flow in focus unaffected from the boundary condition. The flow approaches the wing at an angle of attack of 4° and a Reynolds number, based on the chord length, of $Re = 80000$.

The computational mesh is based on hierarchical refinement of hexahedral cells towards the wing surface. Hanging nodes are avoided by inserted polyhedral cells in the interface region between the different refinement levels. For an appropriate resolution of the boundary layer in wall normal direction, cell layers are placed immediately on the surface ensuring y^+ well below unity in the first cell and a smooth transition towards the surrounding mesh. Figure 1 illustrates the coarsest of the involved meshes. Leading edge and trailing edge are refined further than the central part of the wing in order to capture the strong gradients upstream of the stagnation point and the geometric features of the slightly blunt trailing edge. The phenomena of separation, transition and re-attachment all take place in the uniformly resolved part between these refined zones.

All meshes follow the same structure but feature different levels of refinement on the wing surface. The cell width parallel to the wall is doubled in each step of coarsening. The normal resolution, whereas, is similar as the criterion of y^+ should not be violated. Thereby the number of cell layers to match the surrounding mesh decreases for the finer meshes. Consequently, the non-dimensionalized cell width x^+ and z^+ also also follows a factor of two between the meshes. Since the mesh is based on equilateral hexahedra, x^+ and z^+ have approximately the same value. The values for all meshes are provided by Table 1. Only Meshes 1 to 4 have also been applied for two-dimensional URANS as Mesh 4 already is too coarse. The 2D mesh is directly derived from the three-dimensional meshes, it consists of the periodic boundary plane.

Table 1: Key figures of the involved meshes (cell width Δ/c, non-dimensionalized width x^+, y^+, z^+ of first cell layer).

		Δ/c	y^+	x^+, z^+
Mesh 1	2D,3D	$1/2048$	< 0.4	1.6
Mesh 2	2D,3D	$1/1024$	< 0.4	3.0
Mesh 3	2D,3D	$1/512$	< 0.5	6.3
Mesh 4	2D,3D	$1/256$	< 0.25	10.9
Mesh 5	3D	$1/128$	< 0.5	21.8
Mesh 6	3D	$1/64$	< 0.7	43.6

The values of x^+ and z^+ may appear rather small and already suitable for a DNS. However, the common criteria as for example provided by Piomelli & Chasnov (1996) are formulated for a fully turbulent boundary layer. In the present case, the resolution of gradients around flow separation and throughout the transition is the key factor and it will be shown that these phenomena require an even finer grid spacing.

All simulations have been performed using the OpenFOAM flow solver toolbox. The filtered or averaged Navier-Stokes equations are considered in an incompressible formulation and discretized with the finite volume method. Pressure and velocity are coupled in a PISO loop with iterative time-advancement. The discretization is of second order accuracy in space and time. For time stepping a backward scheme has been used. In the hybrid RANS-LES computations, the convective terms of the momentum equation have been discretized using the linear upwind stabilized transport (LUST) scheme, which blends central discretization with 25% second order upwind for increased robustness. Convective transport in the turbulence model equations has been discretized with the vanLeer TVD scheme. In the DNS, a pure second order central scheme has been applied.

As mentioned above, the turbulence has been modeled with a hybrid RANS-LES approach, namely detached eddy simulation (DES) in the variants delayed DES (DDES) (Spalart *et al.*, 2006) and improved delayed DES (IDDES) (Shur *et al.*, 2008). As underlying RANS model the SST model has been selected featuring two transport equations which in LES mode effectively transform into a one-equation model. Upstream of the transition, the turbulence model needs to be deactivated as otherwise the RANS-modeled turbulent boundary layer would not be able to separate. Only laminar flow will separate under these conditions. Therefore, the γ-Re_θ model according to Langtry & Menter (2009) has been coupled with the *DES approaches. By solving two additional transport equations, the model prescribes transition and activates production of modeled turbulence energy. In a more complex configuration, this approach also could predict transition in an attached boundary layer which, however, would then feature fully modeled turbulence.

In the present setup resolved turbulent structures arise from the shear layer above the separation bubble. The idea behind DES, treating the flow near the wall by RANS and switching towards LES once the turbulent structures can be resolved, requires that this transition zone is located in the LES zone. As will be shown below, DDES fails to resolve the transition process once the grid becomes too coarse. The resulting flow is undefined URANS with a few resolved scales. In this case IDDES, which additionally features a mode of wall modeled LES, still switches into LES and maintains resolved fluctuations in the boundary layer. Therefore the simulations on the coarser grids haven been performed using IDDES, whereas DDES is restricted to the finer meshes.

It should be noted that this application could easily be treated with pure LES and also the DNS has been performed on the same mesh. Hybrid RANS-LES does not necessarily bring

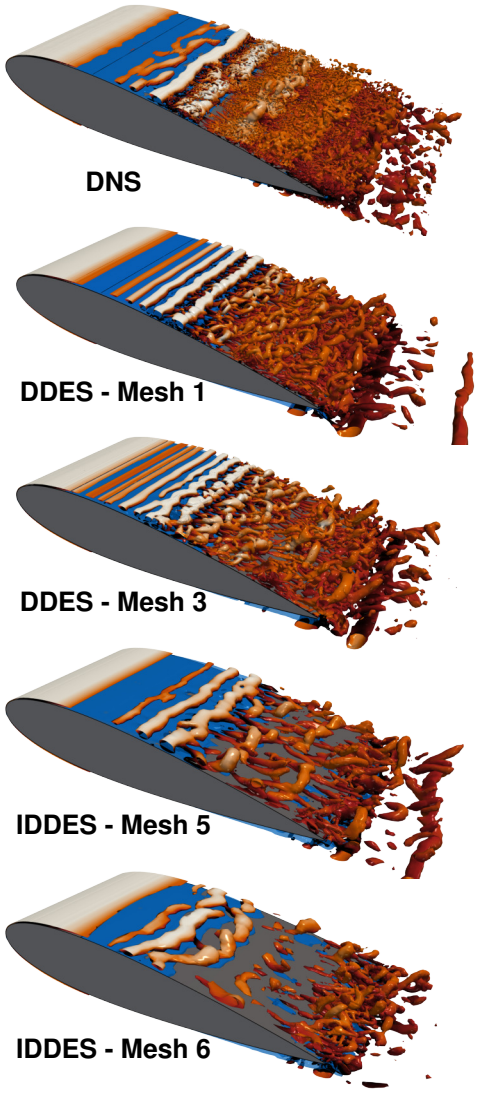

Figure 2: Instantaneous view of the flow field. Iso-surface from Q-criterion colored by stream-wise velocity (white-red) and regions of separated flow (blue).

an advantage in computational efficiency at these conditions of low Reynolds numbers. However, the present setup has been selected precisely because it is possible to perform simulations with all these approaches at bearable computational effort for a detailed comparison before moving to configurations at higher Reynolds number beyond reach for LES and DNS.

In order to separate the effects of refinement between LES and the underlying RANS model, also URANS simulations have been performed. They are kept purely two-dimensional due to the planar nature of the flow. In these cases turbulence is modeled using the SST model with γ-$Re-\theta$ transition modeling exactly as the configuration from the *DES setup.

RESULTS AND DISCUSSION

A first overview to the range of solutions obtained from the different mesh resolutions can be seen from the plots of instantaneous flow features in Figure 2. It shows iso-surfaces from Q-criterion for selected cases together with indications of separated flow regions. All cases produce the general process of separation, transition and re-attachment but with clear deviations. The DNS as a reference shows very fine scales which are not reproduced in the *DES. Considering that DDES on Mesh 1 features an even finer resolution than the DNS, which has been obtained on Mesh 2, this fact needs to be attributed purely to the spatial discretization scheme, which blends in just a small amount of second order upwind in the *DES. The structures of larger scales remain comparable up to Mesh 5. By refining the cells, more and more smaller structures fill the space between the large structures. Mesh 6 clearly approaches the limit of applicability as also the large structures cannot be resolved entirely. Only parts of the characteristic horseshoe vortices are visible in the plot.

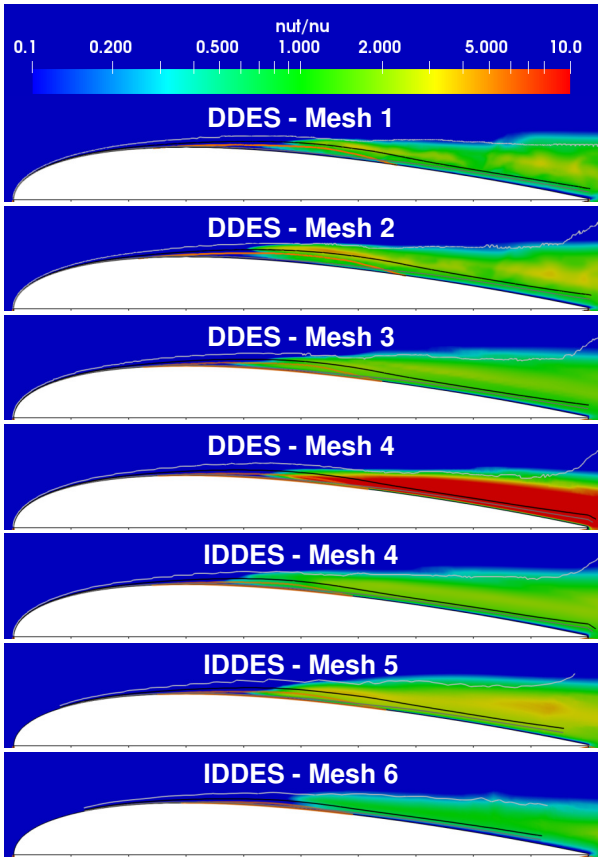

Figure 3: Mean eddy viscosity fields together with boundary layer properties: mean separation bubble (orange), 99%-thickness δ_{99} (light gray), displacement thickness δ^* (black), momentum thickness Θ (dark gray).

Also the transition process shows significant differences between the cases. The finer cases with *DES show shear layer Kelvin-Helmholtz instabilities in very straight lines before they break up into three-dimensional turbulence. The coarser the grid becomes, the sooner this breakup occurs. On the other hand, the DNS also does not show straight vortices. The shear layer instabilities immediately appear slightly wrinkled almost comparable to the coarser meshes.

The effect of the turbulence models on the flow fields can be measured by the levels of eddy viscosity, which is shown in Figure 3 together with properties of the boundary layer. It needs to be noted that the color is scaled logarithmically to also visualize the contributions of different magnitudes. In all cases the model is turned off until after the flow separates. Together with the resolved transition, the sub-grid model also becomes active triggered by the γ-Re_Θ model. Once active, the case of

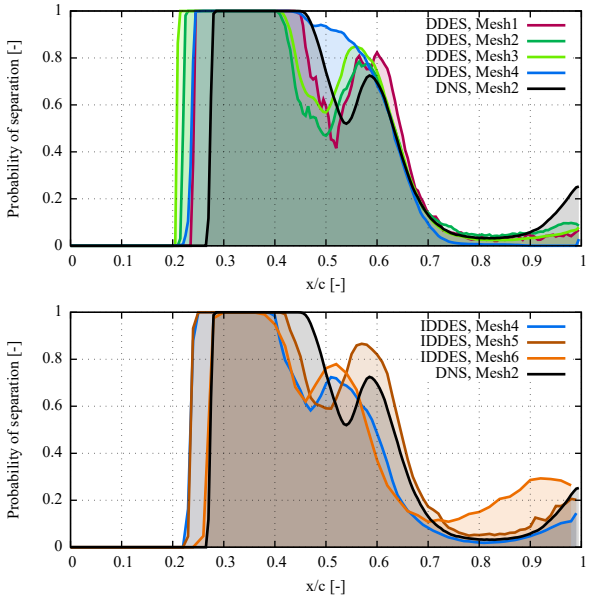

Figure 4: Probability of separated flow along the upper wing surface.

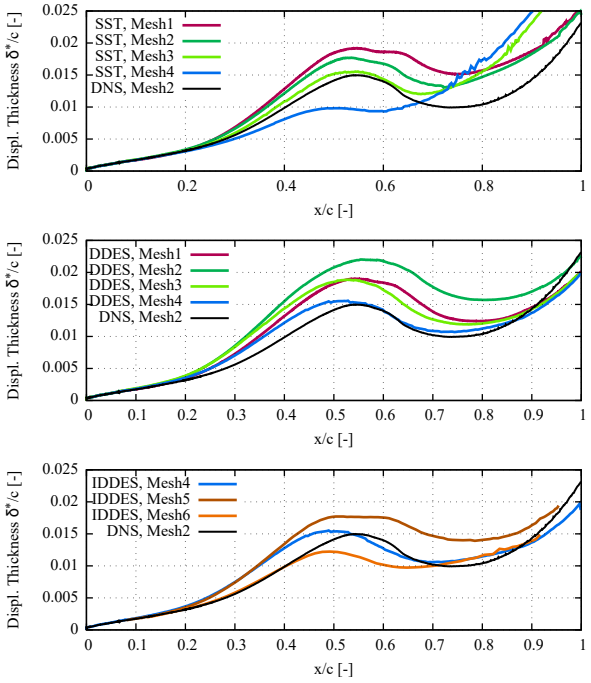

Figure 5: Boundary layer displacement thickness δ^*/c along the upper side of the wing.

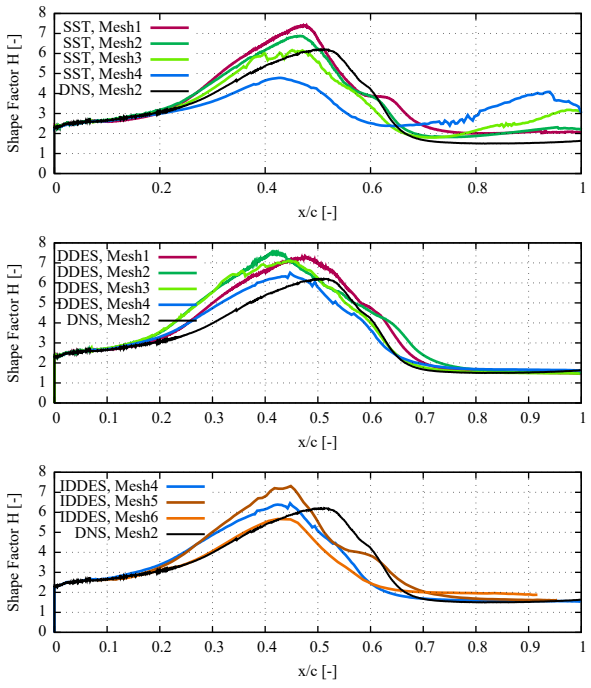

Figure 6: Boundary layer shape factor $H = \delta^*/\Theta$ along the upper side of the wing

DDES on Mesh 4 clearly behaves different as the eddy viscosity is far higher than in the other cases. Here the model goes into URANS mode suppressing resolved turbulent structures by high eddy viscosity.

The other configurations from Mesh 1 to Mesh 4 show very similar levels of eddy viscosity with a slight maximum in the region of the greatest displacement thickness before re-attachment and where the separation bubble becomes thinner. Within the separation bubble eddy viscosity also gets convected upstream leading to the pattern which can be seen in the plots. In Mesh 5 the eddy viscosity is slightly higher as significantly more structures need to be covered by the model. Finally, Mesh 6 brings the IDDES to its limits. The eddy viscosity drops rather low and, as will be shown below, the prediction of the turbulent boundary layer becomes less accurate.

The key feature of this flow is the flow separation which initiates the entire process. In ideally laminar freestream conditions as they can be found in the present setup, the separation occurs in a straight line which is hardly affected by processes further downstream. The re-attachment, however, takes place in turbulent flow and therefore appears very unsteady. In the following turbulent boundary layer, also local separation is present. It can be seen best in the plot from Mesh 6 in Figure 2 as the separated spots are covered but still present in the other plots. Investigating the separation in the mean flow field may become misleading. Instead, Figure 4 shows the time-averaged probability to encounter separated flow along the chord. The initial separation produces a steep rise. Its location varies significantly depending on the configuration. This is not an effect of the turbulence model as it occurs in the laminar region. Actually, this behavior is purely affected by the mesh resolution and, in comparison with DNS, by the discretization scheme, which both change the capability to resolve gradients of pressure and velocity.

After the initial separation, a range of fully separated flow appears in all cases. The first stage of re-attachment is then caused by the growing diameter of the shear layer vortices leading to a decrease of the mean separation probability. Once a vortex breaks up into smaller scales, the trend to re-attach stops, instead the fraction of separated flow increases. When the turbulent boundary layer forms, the probability of separation decays to a every low level but above zero as embedded patches of separated flow are still present. Towards the trailing edge, the trend to separation slightly increases.

This process is produced by most cases. Only the DDES on Mesh 4, which remains in URANS mode, does not predict the dip of separation probability as the breakup into resolved turbulence is missing. Mesh 1 produces a curve closer to the DNS. The other cases up to Mesh 4 show a quantitatively very

similar behavior with the onset of the re-attachment process slightly upstream of the DNS. Also breakup takes place sooner but the turbulent boundary layer is reached in accordance with the DNS. The coarsest Meshes 5 and 6 also show the process but the quantitative deviations are stronger. Mesh 6 shows a significantly higher rate of separated flow within the turbulent boundary layer. The general trend of the *DES cases to predict the onset of re-attachment sooner is supposed to be connected with the observation that the shear layer vortices remain more planar than observed from the DNS. Therefore, they can grow slightly faster and initiate re-attachment before breaking up.

A closer look to the properties of the boundary layer is provided by Figures 5 and 6 showing displacement thickness δ^* and shape factor $H = \delta^*/\Theta$ along the upper side of the wing. Besides results from the turbulence resolving cases, also results from 2D URANS are plotted to give an indication how far the underlying RANS model in the hybrid simulations could provide reasonable results. As long as the flow remains in a mostly two-dimensional structure, the results are in good agreement. Towards the rear part the prediction becomes less accurate. The shape factor of the turbulent boundary layer is significantly mispredicted by URANS. Further can be seen, that with Mesh 4 the URANS is not at all capable of producing the flow process, for which reason no results from coarser meshes have been considered.

In the turbulence-resolving simulations a coarser mesh resolution appears applicable since three-dimensional effects are covered. Even the DDES with Mesh 4, which effectively is close to a 3D URANS, provides better results - of course at a far higher total cell count than all 2D RANS meshes presented here. The general trend in Figure 5 is an overprediction of displacement thickness by *DES compared to the DNS. This, again, is expected to be attributed mainly to the spatial discretization as it already appears far upstream of the model activation. In terms of the shape factor, the attached parts of the laminar and turbulent boundary layers are captured very well. The increase of the shape factor prior to transition occurs slightly upstream of the DNS as could be expected from the sooner separation. The drop towards the turbulent attached part occurs similar to the DNS. The finer meshes tend to show this process further downstream than the coarser ones.

As seen from the quantities discussed above, the transition takes place at slightly different stream-wise locations in the different cases. For a closer investigation of the resolved transition process in a more isolated way, it appears useful to compare the cases with respect to the transition onset point. Several criteria are common in the literature for example based on Reynolds shear stress or boundary layer thickness. Here the location of maximal displacement thickness has been selected as a reference point. It is typically located slightly downstream of the maximum bubble thickness and marks the onset of a steep increase of turbulence. In the following plots, the stream-wise coordinate has been shifted by this length. Table 2 provides the exact locations.

Table 2: Stream-wise coordinate x/c of maximal displacement thickness.

	DNS	DDES	IDDES	2D-URANS
Mesh 1		0.5461		0.5482
Mesh 2	0.5364	0.5572		0.5360
Mesh 3		0.5267		0.5435
Mesh 4		0.5285	0.4894	0.5040
Mesh 5			0.5038	
Mesh 6			0.4920	

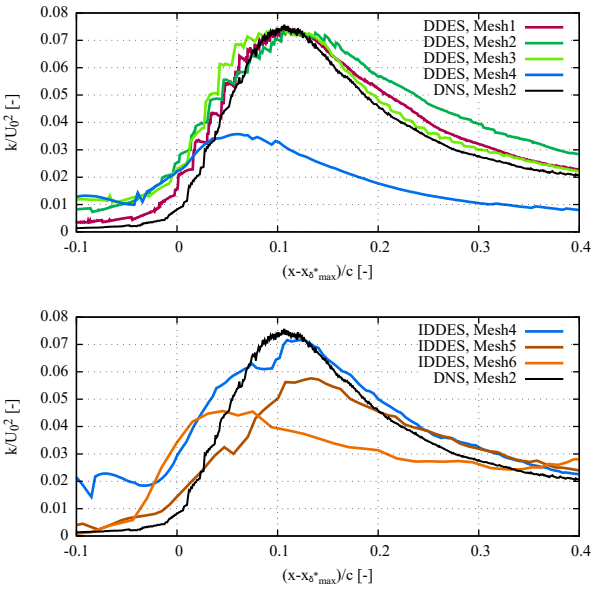

Figure 7: Resolved turbulence kinetic energy $\langle k \rangle$ along the displacement thickness. Stream-wise coordinate shifted with respect to location of maximal displacement thickness.

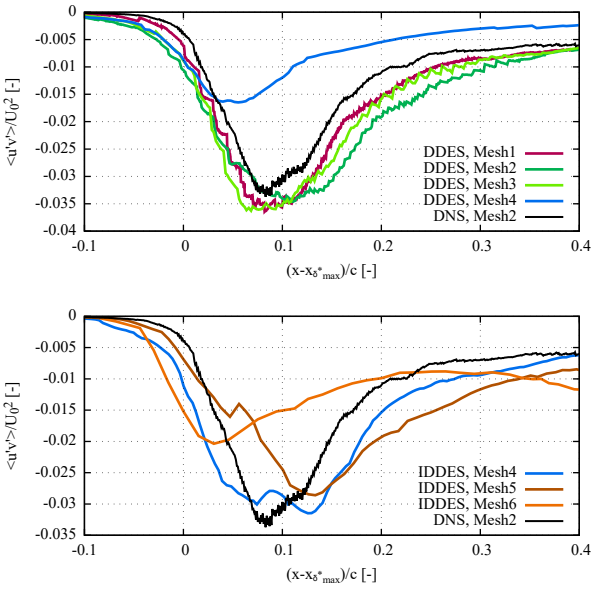

Figure 8: Resolved turbulence shear stress $\langle u'v' \rangle$ along the displacement thickness. Stream-wise coordinate shifted with respect to location of maximal displacement thickness.

Figure 7 shows the resolved turbulence kinetic energy along the displacement thickness. From the DNS, it can be seen that onset of the steep rise coincides well with the maximal displacement thickness. The levels of fluctuation energy

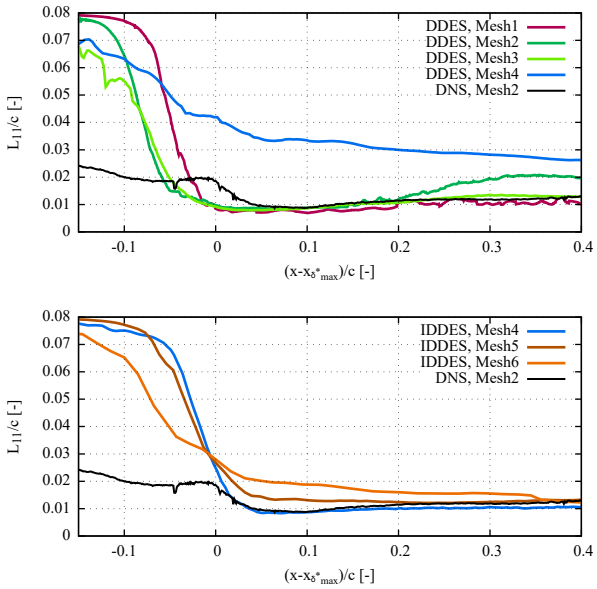

Figure 9: Integral length scale L_{11}/c along the displacement thickness. Stream-wise coordinate shifted with respect to location of maximal displacement thickness.

prior to the reference point are predicted already significantly higher by the *DES than seen from the DNS. The results from Mesh 1 appear slightly better than those from the coarser meshes. Once the flow becomes turbulent, most cases produce a very similar level of resolved fluctuation energy. The DDES Mesh 4 case clearly does not resolve much turbulence. But also from Meshes 5 and 6 a reduction of resolved fluctuations can be seen. Especially Mesh 6 fails as the produced profile appears rather different from the other cases.

A similar view is given by the shear stress $\langle u'v' \rangle$ in Figure 8. It is noteworthy that here all cases start with a value of nearly zero. Besides those cases which do not appropriately resolve the process, all *DES cases first produce a slightly sooner rise of $\langle u'v' \rangle$ towards the greatest magnitude than the DNS. The magnitude then is predicted very well. Finally, the decaying phase is predicted slightly too weak.

From a technical point of view, the small turbulent structures within the boundary layer after transition might be of less interest as long as intensity and size of the larger scales are captured well. A quantity to measure this is the integral length scale. Utilizing the homogeneity of the span-wise direction, the integral length scale L_{11} on the displacement thickness has been computed. Figure 9 shows the resulting profiles with the coordinate conditioned to the maximal displacement thickness as above. Again, the DDES on Mesh 4 produces significantly different results as discussed before. All *DES results exhibit a large length scale in the beginning which drops strongly during transition. The DNS prescribes a similar behavior, but due to its less diffusive discretization and the consequence that the shear layer flow is less planar, the length scale is significantly smaller. It starts dropping once the maximal displacement thickness is reached. This behavior is produced different by the DDES, which at the reference location just reaches the final value of L_{11}. The breakup process towards smaller scales appears to occur later and steeper on the finer grids. The IDDES seems to perform slightly better as at least for the Meshes 4 and 5 the breakup starts further downstream and ends with the DNS. Meshes 5 and 6 are not capable of resolving the scales seen on the finer meshes any more. Within the turbulent boundary layer, the resulting integral length scale is higher. All other cases produce the same L_{11} as the DNS besides some deviation of unclear origin on Mesh 2 towards the trailing edge.

CONCLUSIONS

Simulations of laminar separation on a planar airfoil have been performed using hybrid RANS-LES on a set of six differently fine meshes in order to investigate the effect of mesh resolution on the flow with a particular focus on the transition. In comparison with DNS, it could be shown that not only mesh resolution but also the discretization scheme have a strong influence on the key aspects of the flow, namely separation and transition. The turbulent boundary layer towards the rear part of the wing, however, requires a less fine mesh resolution and allows to apply stability-oriented discretization schemes still obtaining accurate results in terms of resolved turbulence intensity and integral scale of the structures. On the other hand, the front part of the wing needs to be refined very well and should also be treated with accurate schemes.

For future applications this provides chances to increase the efficiency in the simulation of wings at low Reynolds numbers where laminar separation is to be expected. The mesh can be adapted locally to fulfill the required resolution for the different stages of the flow process. It also appears feasible to perform the spatial discretization in a hybrid way to provide best accuracy for the laminar flow and increased stability in the turbulent zones as this is often required especially for more complex geometries.

REFERENCES

Catalano, P. & Tognaccini, R. 2010 Turbulence modeling for low-reynolds-number flows. *AIAA journal* **48** (8), 1673–1685.

Galbraith, Marshall & Visbal, Miguel 2010 Implicit Large Eddy Simulation of Low-Reynolds-Number Transitional Flow Past the SD7003 Airfoil. In *40th Fluid Dynamics Conference and Exhibit*, p. 4737.

Langtry, Robin B & Menter, Florian R 2009 Correlation-based transition modeling for unstructured parallelized computational fluid dynamics codes. *AIAA journal* **47** (12), 2894–2906.

Piomelli, U. & Chasnov, J. R. 1996 Large-eddy simulations: Theory and applications. In *Turbulence and Transition Modelling*, pp. 269–336. Springer Netherlands.

Shur, Mikhail L., Spalart, Philippe R., Strelets, Mikhail Kh. & Travin, Andrey K. 2008 A hybrid RANS-LES approach with delayed-DES and wall-modelled LES capabilities. *International Journal of Heat and Fluid Flow* **29** (6), 1638–1649.

Spalart, P. R., Deck, S., Shur, M. L., Squires, K. D., Strelets, M. Kh. & Travin, A. 2006 A New Version of Detached-eddy Simulation, Resistant to Ambiguous Grid Densities. *Theoretical and Computational Fluid Dynamics* **20** (3), 181–195.

Tangermann, Eike & Klein, Markus 2020 Numerical Simulation of Laminar Separation on a NACA0018 Airfoil in Freestream Turbulence. In *AIAA Scitech 2020 Forum*. American Institute of Aeronautics and Astronautics.

Tangermann, Eike & Klein, Markus 2021 Numerical simulation of a separating laminar boundary layer exposed to ambient turbulence. In *14th WCCM-ECCOMAS Congress*. CIMNE.